Influence of clutch tribodynamics on drivetrain noise, vibration and harshness, (NVH), phenomena

Influence of clutch tribodynamics on drivetrain Noise, Vibration and Harshness, (NVH), phenomena

Author, co-author (Ilias Minas[1], Nicholas Morris[1], Martin O'Mahony[2] and Stephanos Theodossiades[1])
Affiliation (Loughborough University[1] ,Ford Motor Company Ltd[2])

Abstract

Limiting problematic Noise, Vibration and Harshness (NVH) phenomena in the modern automotive drivetrain is a task of critical importance. The result of such phenomena is the aggravation of the driver, which results in a reduced perception of vehicle quality. Each phenomenon can be characterized by a distinct frequency range. The aim of the current study is to assess the influence of the interfacial frictional behavior of the dry friction clutch components on the drivetrain dynamic behavior. The dynamics of the system (in terms of its stability) are studied. Surface data from the clutch components are critical to understanding the complex engagement process. The coefficient of friction was measured using a rotary tribometer at representative slip speeds and contact pressures. To aid the analysis infinite focus microscopy was used to measure the geometric properties of the constituent components of the drivetrain. The current approach allows for improved understanding of the drivetrain's dynamic behavior. The improved understanding of the coupling between tribological characteristics and drivetrain system dynamics can lead to the mitigation of future NVH issues.

Introduction

The development of the modern automobile must consider multivariate design objectives including: efficiency, performance and driver comfort. These design objectives frequently present contradictory design requirements. The automotive industry conforms to strict emission regulations by reducing vehicle weight through: engine downsizing, reductions in component size and the introduction of lightweight materials. This new range of lightweight and highly efficient vehicle drivetrains has not been without consequence. The reduction of component weight has often led to higher levels of Noise, Vibration and Harshness (NVH) [1].

NVH phenomena are crucial issues in the modern automotive industry. The vehicle's NVH performance directly affects customer's perception and has direct impact on warranty costs and driver comfort. As a result significant expense and effort is dedicated to improving NVH performance and new design methods to mitigate against future NVH issues [2,3]. To achieve this ambitious goal, the dynamic behavior and interaction of a vehicle's complex subsystems must be fully understood.

NVH phenomena can be classified according to vehicle's operating conditions, sound type, as well as sound and vibration source. For the latter, NVH can be classified as orginating from: high-speed wind, noise, road noise, tire noise, intake and exhaust noise, powertrain noise and ancillary components [4]. In most cases the undesired noise in the vehicle's cabin frequently originates from the powertrain, which is a complex source of noise and vibration because it consists of a large number of sub-systems containing numerous components; each with their own kinematic, dynamic and material dependent behaviors, which can generate specific noises during vehicle operation [5].

An important system of the powertrain is the clutch, which is responsible for the transmission of power from the engine to vehicle's gearbox. The clutch system is located between the flywheel and the gearbox and since it consists of various moving / interacting parts, it is a potential source of NVH phenomena. Additionally, during its operation (engagement-disengagement) many properties of the interface such as pressure, material properties and sliding velocity vary and as a result so does the coefficient of friction. The vibration generated in this sub-system influences the driveline vibrations and noise reaching driver's ears in the vehicle cabin. This has driven research on vibrations that arise during clutch operation in order to prevent poor ride quality, discomfort and vehicle noise. Common unwanted clutch issues include judder, eek and whoop.

Previous studies have been conducted to explore the effect of friction coefficient on clutch system stability. Wickramarachi and Trinh [6,7] created a clutch model, combining the bending motion of the pressure plate and clutch disc with the axial motion of the pressure plate. Stability analysis was conducted concluding that an increasing coefficient of friction creates instability in the mechanical system. Moreover, the pressure plate's stiffness and inertia affect the system vibrations. Fidlin [8] conducted a numerical study on dry clutch friction disc dynamic behaviour. A clutch system model with gyroscopic terms and friction induced damping was used for stability analysis. The relation between the friction coefficient and the internal structural damping was made and the analytical results were compared to results of numerical simulation.

Ghorbel et. Al. [9] designed a general dynamic model for the whole drivetrain. He divided the drivetrain in different sections (clutch, gearbox and disc brake) and modelled each separately. For every model the kinetic and strain modal energy distribution was examined. The dynamic model of the clutch system consists of the flywheel and cover, friction disc, hub and pressure plate. All of which were connected with torsional springs. Proportional damping was used and a modal analysis was conducted after parametric change for coefficient of friction and the stiffnesses. It was found that the torsional stiffness significantly affects stability of the system.

Crowther [10] developed a 4 degree of freedom torsional model of the clutch system along with the engine and the gearbox. The stick slip

behaviour during clutch engagement was examined. Stability analysis proved that the gradient of the friction coefficient curve, affects the excitation that leads to judder. Numerical simulations confirmed the mathematical model, after building an algorithm for the demonstration of the stick slip behaviour.

The aim of the current study is to assess the influence of dry friction characteristics of clutch components on drivetrain dynamic behavior. Surface specific data from the clutch components are critical to understanding the complex engagement/disengagement process. The coefficient of friction is measured at representative slip speeds and clamp loads. The surface features and the geometric properties of the constituent components were assessed with the use of focus variation microscopy and a coordinate measuring machine. The current method allows for improved understanding of the clutch dynamic behavior and coupling between tribological characteristics and system dynamics that can potentially lead to mitigation of NVH.

Methodology

The methodology presented herewith comprises a dynamic clutch model that includes translational and torsional motions of the clutch components. Modal analysis was conducted to calculate the natural frequencies of the system, mode shapes and the stability properties. The friction coefficient is an essential input parameter which affects the stability of the system. The experimental methodology for the measurement of coefficient of fiction is discussed later in the paper.

Clutch model

The clutch model (figure 1) has 6 degrees of freedom (DOF), describing the torsional and axial motion of the clutch components.

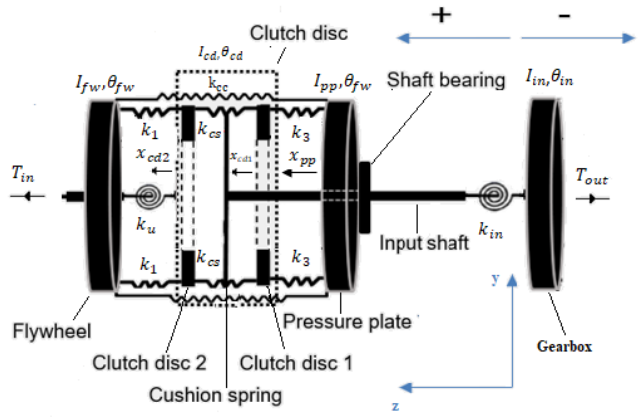

Figure 1. Dry clutch schematic representation - dynamic model

The clutch model is characterized by the following vector of generalized coordinates:

$$\boldsymbol{q} = \{\boldsymbol{\theta_{fw}}, \boldsymbol{\theta_{cd}}, \boldsymbol{\theta_{in}}, \boldsymbol{x_{pp}}, \boldsymbol{x_{cd1}}, \boldsymbol{x_{cd2}}\} \quad (1)$$

In which:

θ_{fw}: *rotation of flywheel and pressure plate around z axis*
θ_{cd}: *rotation of the clutch disc around z axis*
θ_{in}: *rotation of gearbox and input shaft around z axis*
x_{pp}: *axial displacement of the pressure plate*
x_{cd1}: *axial displacement ofclutch disc* 1
x_{cd2}: *axial displacement of clutch disc* 2

The set of equations of motion for the clutch system is as follows.

Flywheel and pressure plate:

$$(I_{fw} + I_{pp})\ddot{\theta}_{fw} + k_u(\theta_{fw} - \theta_c) + c_1(\dot{\theta}_{fw} - \dot{\theta}_{cd}) = T_{in} - T_c \quad (2)$$

Clutch disc:

$$(I_{cd})\ddot{\theta}_{cd} + k_{in}(\theta_{cd} - \theta_{in}) + k_u(\theta_c - \theta_{fw}) + c_2(\dot{\theta}_c - \dot{\theta}_{in}) = T_c \quad (3)$$

Gearbox input shaft:

$$(I_{in})\ddot{\theta}_{in} + k_{in}(\theta_{in} - \theta_c) + c_3(\dot{\theta}_{in} - \dot{\theta}_c) = -T_{out} \quad (4)$$

Pressure plate:

$$m_{pp}\ddot{x}_{pp} + 2k_3(x_{pp} - x_{cd1}) + 2k_{cc}x_{pp} + c_4(\dot{x}_{pp} - \dot{x}_{cd1}) = F_{sb} \quad (5)$$

Clutch disc 2:

$$m_{cd2}\ddot{x}_{cd2} + 2k_1x_{cd2} + 2k_{cs}(x_{cd2} - x_{cd1}) + c_5(\dot{x}_{cd2} - \dot{x}_{cd1}) = 0 \quad (6)$$

Clutch disc 1:

$$m_{cd1}\ddot{x}_{cd1} + 2k_3(x_{cd1} - x_{pp}) - 2k_{cs}(x_{cd2} - x_{cd1}) + c_6(\dot{x}_{cd1} - \dot{x}_{pp}) = 0 \quad (7)$$

The terms in the equations of motion are:

I_{fw}: *Moment fo flywheel inertia at mass centre*

I_{pp}: *Moment of pressure plate inertia at mass centre*

I_{cd} : *Moment of clutch disc inertia at mass centre*

I_{in}: *Moment of gearbox inertia at mass centre*

m_{pp}: *Pressure plate mass*

m_{cd1}: *Clutch disc facing* 1 *mass*

m_{cd2}: *Clutch disc facing* 2 *mass*

k_{cc}: *Pressure plate cover axial stiffness*

k_{cs}: *Cushion spring axial stiffness*

k_{in}: *Input shaft torsional stiffness*

k_3: *Contact stiffness between clutch disc and pressure plate*

k_1: *contact stiffness between clutch disc and flywheel*

T_{in}: *Engine input torque*

T_c: *Friction torque*

T_{out}: *Torque transmitted to the rest of the vehicle*

F_{sb}: *Clamp load force*

c_{1-6}: *Damping coefficients*

The following assumptions were made:

The pressure plate is connected with the flywheel using the axial spring k_{cc}[11], and both have the same torsional degree of freedom. I The flywheel and clutch disk rotate together [2].

The clutch disc was divided into two parts with the same mass and inertia. These discs are connected elastically by an axial spring, which represents the cushion spring between the two facings of the clutch disc (clutch disc 1 and clutch disc 2).

Friction torque and coupling of motions

The clutch is used for the transmission of the engine torque to the rest of the drivetrain. When the surface of the clutch disc is in contact with the flywheel and the pressure plate, friction enables the transmission of the engine torque. Assuming uniform pressure, T_c is given by [12]:

$$T_c = N_s R \mu_s F \tag{9}$$

N_s is the number of surfaces that are in contact, F is the load that is applied from the shaft bearing (see fig. 1), R is the effective radius of the clutch disc and μ_s is the coefficient of sliding friction. The effective radius of the clutch disc can be calculated as [13,14]:

$$R = \frac{2}{3}\frac{r_o^3 - r_{in}^3}{r_o^2 - r_{in}^2} \tag{10}$$

Where r_o is the outer radius of the clutch disc and r_{in} is the inner radius of the disc facing surfaces.

The friction force couples the rotational and axial motions. Using the gradient (m_s) from friction coefficient measurements and the intercept of the linear fit at zero slip speed (μ_{s0}), the sliding coefficient of friction (μ_s) can be derived using the following [10]:

$$\mu_s = \mu_{s0} + m_s(\dot{\theta}_{fw} - \dot{\theta}_{cd}) \tag{11}$$

As a result, the clutch torque is given by:

$$T_c = N_s R \mu_{s0} F + m_s(\dot{\theta}_{fw} - \dot{\theta}_{cd}) N_s R F \tag{12}$$

The system of equations (2-8) can be written now in the following form:

$$(I_{fw} + I_{pp})\ddot{\Theta_{fw}} + k_u(\theta_{fw} - \theta_c) + (c_1 + m_s N_s RF)(\dot{\theta}_{fw} - \dot{\theta}_{cd}) = T_{in} - N_s R \mu_{s0} F$$

$$(I_{cd})\ddot{\theta}_{cd} + (k_{in})(\theta_{cd} - \theta_{in}) + k_u(\theta_c - \theta_{fw}) + (c_2 + m_s N_s RF)(\dot{\theta}_{cd} - \dot{\theta}_{in}) = N_s R \mu_{s0} F$$

$$(I_{in})\ddot{\theta}_{in} + (k_{in})(\theta_{in} - \theta_c) = -T_{out}$$

$$m_{pp}\ddot{x}_{pp} + 2k_3(x_{pp} - x_{cd1}) + 2k_{cc}x_{pp} + c_4(\dot{x}_{pp} - \dot{x}_{cd1}) = F_{sb}$$

$$m_{cd2}\ddot{x}_{cd2} + 2k_1 x_{cd2} + 2k_{cs}(x_{cd2} - x_{cd1}) + c_5(\dot{x}_{cd2} - \dot{x}_{cd1}) = 0$$

$$m_{cd1}\ddot{x}_{cd1} + 2k_3(x_{cd1} - x_{pp}) - 2k_{cs}(x_{cd2} - x_{cd1}) + c_6(\dot{x}_{cd1} - \dot{x}_{pp}) = 0$$

The governing equations of motion are put in matrix form as below:

$$[M]\{\ddot{X}\} + [C]\{\dot{X}\} + [K]\{X\} = \{F\} \tag{13}$$

Where the mass and stiffness matrices are given by:

$$[M] = \begin{bmatrix} I_{fw} + I_{pp} & 0 & 0 & 0 & 0 & 0 \\ 0 & I_{cd} & 0 & 0 & 0 & 0 \\ 0 & 0 & I_{in} & 0 & 0 & 0 \\ 0 & 0 & 0 & m_{pp} & 0 & 0 \\ 0 & 0 & 0 & 0 & m_{cd2} & 0 \\ 0 & 0 & 0 & 0 & 0 & m_{cd1} \end{bmatrix}$$

$$[K] = \begin{bmatrix} k_u & -k_u & 0 & 0 & 0 & 0 \\ -k_u & k_{in} + k_u & -k_{in} & 0 & 0 & 0 \\ 0 & -k_{in} & k_{in} & 0 & 0 & 0 \\ 0 & 0 & 0 & 2k_3 + 2k_{cc} & 0 & -2k_3 \\ 0 & 0 & 0 & 0 & 2k_1 + 2k_{cs} & -2k_{cs} \\ 0 & 0 & 0 & -2k_3 & -2k_{cs} & 2k_1 + 2k_{cs} \end{bmatrix}$$

Damping coefficients

For the stability analysis of the damped system, the structural damping coefficients were calculated based on proportional damping. The matrix of damping coefficients can be expressed as a combination of the mass and stiffness matrix.

$$[C] = a[M] + \beta[K] \tag{14}$$

In which a and β are constants. The assumption that internal damping is very low leads to $a = 0$. Thus, equation (13) leads to:

$$[C] = \beta[K] \tag{15}$$

Thus, the damping matrix coefficients can be calculated using:

$$2\zeta_n\omega_n = \beta\omega_n^2 \tag{16}$$

ζ_n is the damping ratios and ω_n are the natural frequencies.

The eigenproblem was solved:

$$|K - \lambda M| = 0 \tag{17}$$

In which $\lambda = \omega_n^2$

The eigenvectors are given by:

$$[K - \lambda M]\bar{\varphi} = 0 \tag{18}$$

If any of the real parts of the eigenvalues are positive numbers the system is unstable. For stability analysis the following equation is used after assuming a vector solution of the form:

$$x = \vec{C}e^{st} \tag{19}$$

Which leads to the equation below:

$$([M]s^2 + [C]s + [K])\vec{C}e^{st} = 0 \quad (20)$$

The characteristic equation is calculated by:

$$D(s) = |([M]s^2 + [C]s + [K])| = 0 \quad (21)$$

The above equation leads to the complex eigenvalues of the damped system [15].

Sample preparation and experimental procedure

The kinetic coefficient of friction between two materials that are in contact depends on parameters, such as the relative speed between the contiguous surfaces, contact pressure and the surface topography of each material [16,17]. The aim of the experimental procedure was the emulation of clutch engagement conditions (clamp load and flywheel speed) using the pin on disc rig shown in figure 2. The tribometer comprises: AC motor which transmits torque to the driven disc (2). The disc is a replica of the pressure plate manufactured from mild steel. The disc finish matches the radially sinusoidal form of the pressure plate surface. The wave pattern of the surface roughness has amplitude of approximately 300μm and wavelength of 1mm (figure 3).

The tribometer includes a clutch disc sample (3) that is attached to an arm (5) instrumented with a strain gauge rossete (4). The normal contact load is applied to the arm at point 6 and calibration was made in order to measure the tangential applied force transmitted from the clutch disc sample on the driven disc. The measurements were conducted according to the standard test procedures set out in ASTM G99 or DIN 50324 [18].

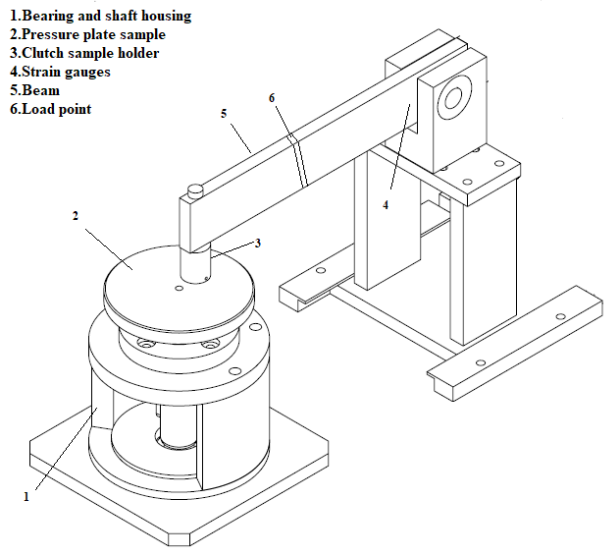

Figure 2. Schematic presentation of pin on disc tribometer

The experimental procedure was conducted for 12 different samples, extracted from a clutch disc facing. The number of random samples from clutch disc's surface which should be tested for representative assessment of the coefficient of friction was calculated using equation [19]:

$$n \geq \frac{(Z*V_x)^2}{e^2} \quad (22)$$

n is the sample size, Z=1.96 is a critical value for 95% confidence level, V_x is the variance of the friction coefficient and e is a value set by investigator.

The mean value of friction coefficient under a specific condition (1200 N and 1200 rpm) and its standard deviation was assessed after testing some samples using the rig of figure 2. Their values were 0.35 and 0.037, respectively. The e value was set in such a way so that the friction coefficient of each sample does not differ from the friction coefficient of the whole clutch disc's area more than ±0.02. Using equation (22) the number of samples required is approximately 12.

The equivalent conditions for in situ clutch clamp load and rotational slip speed that were represented by the experimental procedure are described in tables 1 and 2.

According to ASTM G115-10, in order to compare the coefficient of friction in each condition, the same sliding distance for every sample must be applied [20]. For this study the sliding distance (150m) was selected to limit the effect of frictional heat generation on the bulk temperature of the sliding components. This ensured the changes in the coefficient of friction were a function of sliding speed and load only.

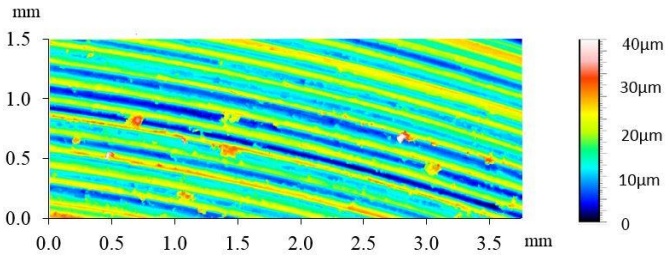

Figure 3. Surface topography snapshot of the rotating disc

Table 1. Experimental conditions (constant sliding speed - clamp load variation)

Sliding speed (rpm)	Time (s)	Clutch clamp load (N)
1200	15.95	400
1200	15.95	800
1200	15.95	1200
1200	15.95	1600
1200	15.95	2000
1200	15.95	2400

Table 2. Experimental conditions (constant clamp load and sliding speed variation)

Clutch clamp load (N)	Time (s)	Sliding speed (rpm)
1200	15.95	1200
1200	14.21	1300
1200	13.2	1400
1200	12.32	1500
1200	11.55	1600
1200	10.87	1700

Before every test cleaning of the pressure plate replica was performed (ASTM G99-05). The surface roughness is an important factor for assessing the friction coefficient value [21, 22], thus before every

measurement the surface topography of each sample and pressure plate's replica were measured using an optical interferometer.

Results and discussion

The stability of the clutch system was investigated using the dynamic model. A nominal case based on a list of typical parameters was selected. Then, a parametric study of the system's stability was performed including the coefficient of friction. Table 3 describes typical ranges of mass, inertia and stiffness properties of the clutch system examined.

Table 3. Range of input parameters of the examined clutch system

I_{fw}	0.1 – 0.2 $kg\ m^2$
I_{pp}	0.03 – 0.05 $kg\ m^2$
I_{cd}	0.004 – 0.006 $kg\ m^2$
I_{in}	0.006 – 0.008 $kg\ m^2$
m_{pp}	4 - 5 kg
m_{cd1}	0.6 – 0.8 kg
m_{cd2}	0.6 – 0.8 kg
k_{cc}	12 10^6 - 14 10^6 N/m
k_{cs}	1.4 10^6 – 1.6 10^6 N/m
k_{in}	30 10^3 - 50 10^3 Nm/rad
k_3	2 10^6 - 3 10^6 N/m
k_1	2 10^6 - 3 10^6 N/m
k_u	70 10^3 - 85 10^3 Nm/rad

The natural frequencies of the system and the corresponding mode shapes are as follows (the coupling between rotational and axial motions is established when the friction force is added):

$$f = \begin{pmatrix} 0 & 0 & 0 & 0 & 0 & 0 \\ 0 & 298.54 & 0 & 0 & 0 & 0 \\ 0 & 0 & 359.46 & 0 & 0 & 0 \\ 0 & 0 & 0 & 492.11 & 0 & 0 \\ 0 & 0 & 0 & 0 & 654.2 & 0 \\ 0 & 0 & 0 & 0 & 0 & 825.03 \end{pmatrix} Hz$$

$$\varphi = \begin{pmatrix} 2.4583 & 0.6450 & 0 & 0 & 0 & 0.2696 \\ 2.4583 & -3.6940 & 0 & 0 & 0 & -13.5731 \\ 2.4583 & -10.7813 & 0 & 0 & 0 & 3.3779 \\ 0 & 0 & -0.3688 & -0.2920 & -0.1184 & 0 \\ 0 & 0 & -0.4035 & 0.8195 & -0.7642 & 0 \\ 0 & 0 & -0.6600 & 0.4826 & 0.8660 & 0 \end{pmatrix}$$

Parametric study

Figure 4 depicts the relation of measured coefficient of friction to clamp load. The slope of the kinetic friction coefficient is positive with clamp load, indicating that when increasing the applied load the coefficient of friction increases under constant sliding speed. Figure 5 shows that for constant clamp load and increase of the sliding speed, the gradient is negative, meaning that the coefficient of friction decreases. A negative slope has been shown to indicate a tendency to judder [14].

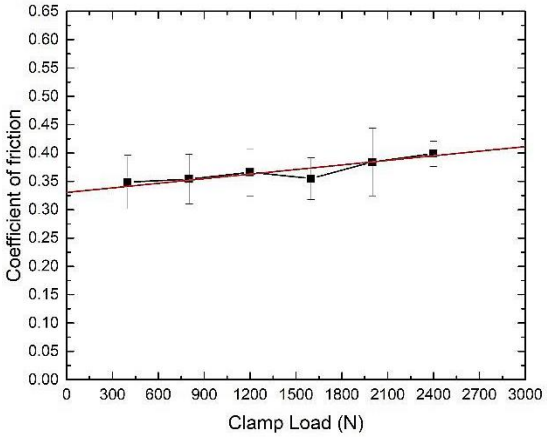

Figure 4. Coefficient of friction vs clamp load under constant sliding speed

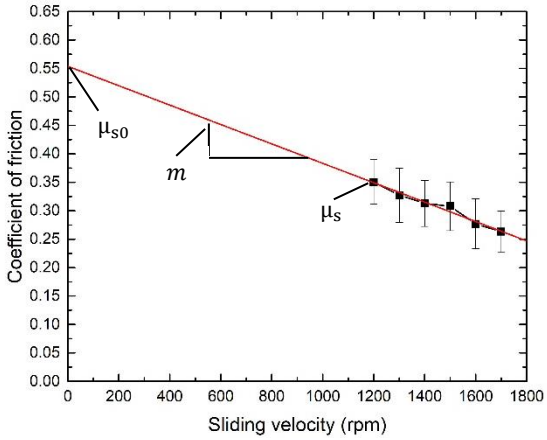

Figure 5. Coefficient of friction vs sliding speed under constant clamp load

The following gradient values of the coefficient of friction have been obtained and are used for the stability analysis.

CoF vs sliding speed gradient	***CoF vs clamp load gradient***
-1.70515E-4	2.69729E-5

The value of the gradient that was used for the stability analysis as a nominal case was -1.70515E-4.

Figure 6 shows the change of (proportional) damping ratio versus natural frequencies with a starting value of 0.0005 (nominal case), which is typical for metallic structures. The damping ratios for higher natural frequencies were calculated using the same β coefficient.

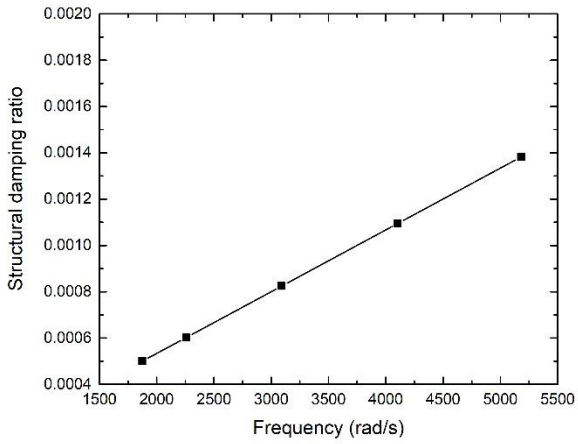

Figure 6. Damping ratios for each natural frequency

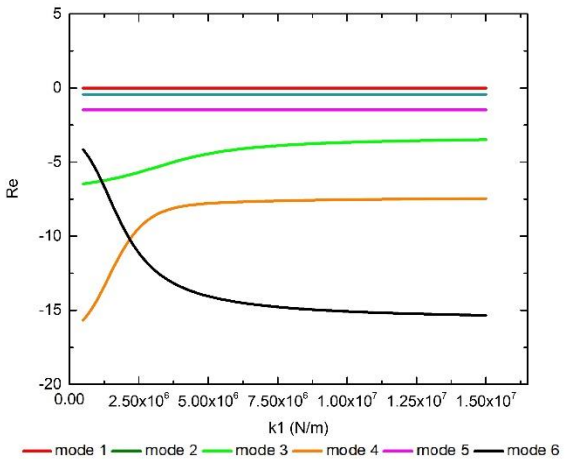

Figure 7. Real parts of eigenvalues vs k_1 axial stiffness

The corresponding damping matrix is as follows:

$$[C] = \begin{bmatrix} 0.0039 & -0.0039 & 0 & 0 & 0 & 0 \\ -0.0039 & 0.0039 & -0.0213 & 0 & 0 & 0 \\ 0 & -0.0213 & 0.0213 & 0 & 0 & 0 \\ 0 & 0 & 0 & 168.78 & 0 & -2.93 \\ 0 & 0 & 0 & 0 & 4.53 & -1.59 \\ 0 & 0 & 0 & -2.93 & -1.59 & 4.53 \end{bmatrix} \begin{matrix} \} \text{N/m} \\ \\ \\ \} \text{Nms/rad} \\ \\ \end{matrix}$$

Table 4 shows the eigenvalues for the nominal case. Moreover, the value for the gradient m_s was taken from the experimental results.

Table 4. Eigenvalues of the damped system for the nominal case

Real parts	***Imaginary parts (rad/s)***	***Frequency (Hz)***
0	0	0
-0.4262	±1874.9	298.54
-11.699	±2257.4	359.46
-9.0266	±3090.46	492.11
-5.5564	±4108.4	654.2
-1.4712	±5181.23	825.03

It can be concluded that the system is stable for this set of parameters. The parametric study of the system's stability will be shown in the graphs below. Figure 7 presents the real part of the complex eigenvalues when changing the axial contact stiffness (k_1) between the flywheel and clutch disc 2.

For the selected range of axial contact stiffness (k_1) all the modes have negative real values. As a result, the system remains stable. The most affected mode due to this change is mode 6 which clearly decreases with the increase of the stiffness value. Mode 4 is also affected by increasing fast in the beginning but after a threshold value it increases slightly. Figure 8 shows the effect that the torsional stiffness between the clutch disc and the flywheel has on the stability of the system.

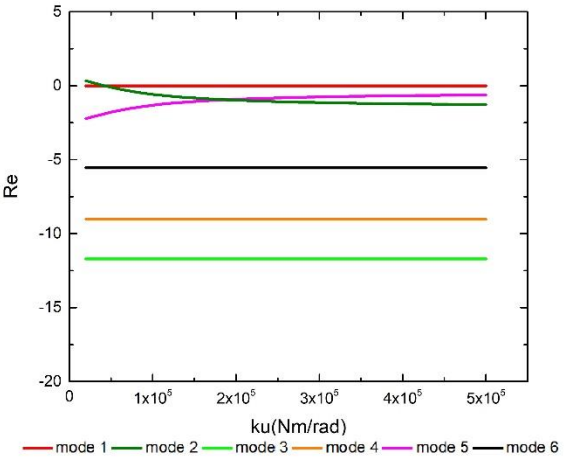

Figure 8. Real parts of eigenvalues vs k_u torsional stiffness

The main observation that can be made is that for smaller values of torsional stiffness k_u, the system is unstable. Mode 2 creates this instability. As the stiffness values increase though this mode becomes stable. The real part of mode 5 tends to increase slowly with the increase of the torsional stiffness. Figure 9 shows the effect that input shaft's torsional stiffness has on the stability of the system.

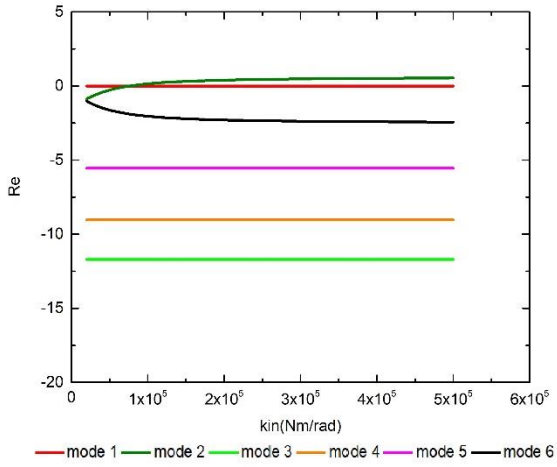

Figure 9. Real parts of eigenvalues vs k_{in} torsional stiffness

For small values of input shaft's torsional stiffness, the system remains stable. The real part of mode 2 starts increasing and quickly leads the system to instability. On the other hand, figure 10 presents the effect of cushion spring's axial stiffness on system's stability. All the modes have negative real parts, so the system remains stable for this range of values for cushion spring stiffness. The real parts of modes 3 and 5 have a small increase but as the stiffness value increases they remain stable with negative real parts.

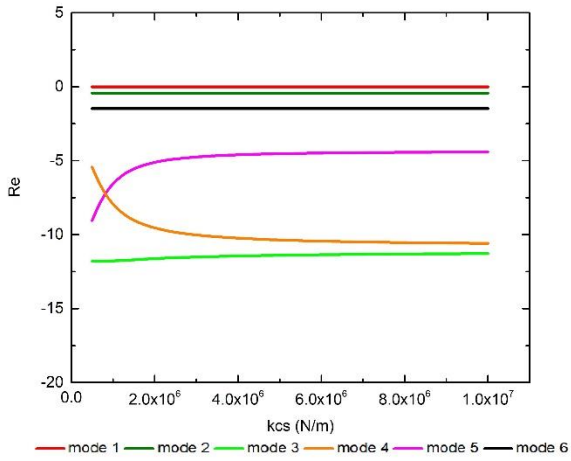

Figure 10. Real parts of eigenvalues vs k_{cs} axial stiffness

Figure 11 shows the effect that the axial stiffness of pressure plate cover on the stability of the system. It can be observed that all the modes have negative real parts of the eigenvalues for the selected range and thus, the system remains stable. Finally, figure 12 shows the effect that clamp load has on the stability of the system. With the increase of clamp load above 2000 N the system becomes unstable due to modes 2 and 6. Using equation (9), which describes friction torque created due to the contact of clutch disc with the pressure plate and flywheel, it can be seen that the clamp load influences the coefficient of friction. Figure 4, shows the effect that clamp load has of the coefficient of friction. Applying higher clamp loads leads to the increase of the coefficient of friction. Finally, equation (9) shows that in higher clamp loads, the coefficient of friction is higher and as a result, the friction torque increases. This means that the system is closer to full engagement.

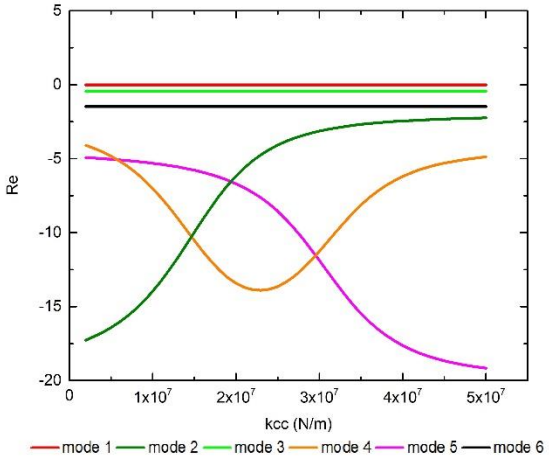

Figure 11. Real parts of eigenvalues vs k_{cc} axial stiffness

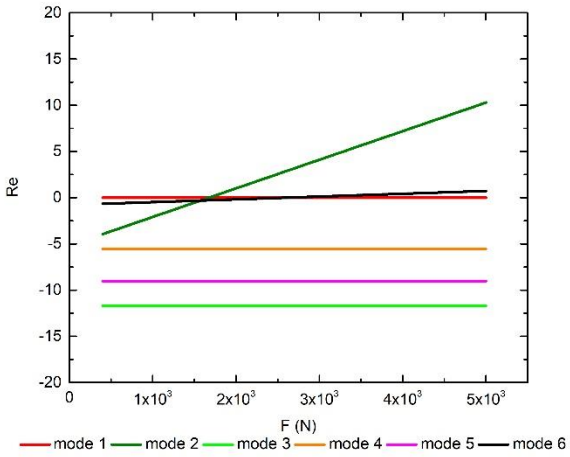

Figure 12. Real parts of eigenvalues vs c*lamp load*

Modal analysis was conducted to explore the response of the system due to variations in the kinetic coefficient of friction. A change in the sliding coefficient of friction (μ_s) leads to alternation of the linearized curve's gradient (figure 5). In tables 5, 6 the eigenvalues are presented, for two different values of the sliding coefficient of friction (μ_s) .These values were higher, compared to those observed in the experiments, so that the effect of coefficient of friction's variation to system's stability be assessed. The data presented in tables 5, 6 reveal that the increase of the coefficient of friction has negative impact on system's stability. Thus, the combination of high magnitude and gradient of the coefficient of friction lead the system towards instability. In both cases mode 6 has a positive real part, revealing instability of the system.

Table 5. Real parts of the eigenvalues with higher sliding coefficient of friction and gradient.

μ_s	***gradient***	***Real parts***
0.40631	-2.49049E-4	-0.25632
0.40631	-2.49049E-4	-11.69
0.40631	-2.49049E-4	-9.026
0.40631	-2.49049E-4	-5.556
0.40631	-2.49049E-4	0.259

Table 6. Real parts of the eigenvalues with higher sliding coefficient of friction and gradient.

μ_s	*gradient*	*Real parts*
0.45167	-2.8910E-4	-0.1730
0.45167	-2.8910E-4	-11.69
0.45167	-2.8910E-4	-9.026
0.45167	-2.8910E-4	-5.556
0.45167	-2.8910E-4	1.1084

Conclusions and future work

The aim of this study was to investigate the effect of the clutch tribodynamics on system's stability. The main system parameters were varied and the following conclusions were made:

- The clamp load creates instability above a threshold value (2000N)
- The contact axial stiffness (k1) between the clutch disc and flywheel does not affect the system's stability. Moreover, the pressure plate cover axial stiffness along with the axial stiffness of the cushion spring has no effect on system's stability either.
- The torsional stiffness of the input shaft can introduce instability (for low values).
- The torsional stiffness between the clutch disc and the flywheel may lead the system to instability.
- The coefficient of friction has a negative impact on system's stability. For higher values of the kinetic friction coefficient the system tends to be more unstable.
- The instabilities appeared in the current study create a noise and vibration with frequency around 298.94 Hz, which corresponds to mode 2 and 825.03 which represents mode 6. The noise has high frequency and can be audible from the driver of the vehicle in the cabin. The instabilities are due to vibrations during clutch disc rotational motion and during input shaft's rotation.

The addition of bending degrees of freedom in the clutch model and transient numerical simulations constitute part of the proposed future work. The model proposed for this study does not combine bending degrees of freedom for simplicity. Moreover, the instabilities created due to the translational and torsional motions of the clutch components can be fully described with the current model, which is the aim of the study.

References

1.Dejan V. Matijević, Vladimir M. Popović. 2017. "Overview of Modern Contributions in Vehicle Noise and Vibration Refinement with Special Emphasis on Diagnostics," 448–58. doi:10.5937/fmet1703448M.

2.Senatore, Adolfo, Daniel Hochlenert, Vincenzo D Agostino, and Utz Von Wagner. 2017. "IMECE2013-64597," 1–9.

3.Young, Shaobo, and D Ph. 2014. "The 21 St International Congress on Sound and Vibration vehicle NVH development process and technologies" no. July: 13–17.

4. Zhao, Xuanming. 2016. "Analysis on Vibration NVH of General Mechanical" 104 (Icmcm): 758–61.

5.Pitchaikani, Anand, Shankar Venkataraman, Kiran Kumar Koppu, John Batteh, and Michael Tiller. 2009. "Powertrain Torsional Vibration System Model Development in Model- Ica for NVH Studies," 20–22. doi:10.3384/ecp09430009.

6.Trinh, M H, S Berger, and E Aubry. 2013. "Non-Intrusive Generalized Polynomial Chaos Takes Uncertain Parameters into Account in the Stability Analysis of a Clutch System Abstract :," 3–8.

7.Wickramarachi, Pierre, Rajendra Singh, and George Bailey. 2005. "Analysis of Friction-Induced Vibration Leading to 'EEK' noise in a Dry Friction Clutch." Noise Control Engineering Journal 53 (4): 138. doi:10.3397/1.2839252

8.Fidlin, Alexander, Olga Drozdetskaya, and Bernd Waltersberger. 2011. "On the Minimal Model for the Low Frequency Wobbling Instability of Friction Discs." European Journal of Mechanics, A/Solids 30 (5). Elsevier Ltd: 665–72. doi:10.1016/j.euromechsol.2011.03.009.

9.Ghorbel, A, M Abdennadher, B Zghal, and L Walha. 2017. "Modal analysis and dynamic behaviour for analytical drivetrain model," 1–17.

10.Crowther, A, N Zhang, D K Liu, and J K Jeyakumaran. 2007. "Analysis and Simulation of Clutch Engagement Judder and Stick – Slip in Automotive Powertrain Systems," no. January 2004: 1427–46.

11.Chen, Xiangbin, Weimin Zhang, and Guoqing Wu. 2016. "A Multi-Body Dynamic Modeling and Experimental Study of EEK Noise During Clutch Engagement." Journal of Failure Analysis and Prevention 16 (6). Springer US: 1052–58. doi:10.1007/s11668-016-0181-3.

12.Yao, Jian, Li Chen, and Chengliang Yin. 2014. "Modeling and Stability Analysis of Wedge Clutch System" 2014.

13.Centea, D. and H. Rahnejat. "The Influence of the Interface Coefficient of Friction upon the Propensity to Judder in Automotive Clutches."

14.Centea, D, and H Rahnejat. 2001. "Non-Linear Multi-Body Dynamic Analysis for the Study of Clutch Torsional Vibrations (Judder)" 25: 177–92.

15. Rao, Singiresu S. n.d. Fifth Edition.

16. Fernandes, G P, P S Zanotto, and A Sinatora. 2015. "Contribution on Understanding the Friction Fi Lm Development in the Performance of a Dry Automotive Clutch System." Wear 342–343. Elsevier: 364–76. doi:10.1016/j.wear.2015.09.007.

17. Abdullah, Oday I, and Josef Schlattmann. 2013. "Contact Analysis of a Dry Friction Clutch System" 2013.

18. Gkinis, T.. "E Ect of Clutch Lining Frictional Characteristics on Take-up Judder," no. June. doi:10.1177/1464419317708946.

19. P.S. Levy, S.Lemeshow. 1991. Sampling of Populations, Methods and Applications. 2nd ed. Singapore.

20. Humphreys, E.. 2016. "Clutch Lining Frictional Characteristics under Thermal Tribodynamic Conditions," 0–11.

21. Bhushan, Bharat. 2001. "2.1 The Nature of Surfaces."

22. Ostermeyer, G P. 2003. "On the Dynamics of the Friction Coefficient" 254: 852–58. doi:10.1016/S0043-1648(03)00235-7.

Contact Information

Ilias Minas
Wolfson School of Mechanical and Manufacturing Engineering
Loughborough University
Loughborough, Leicestershire, LE11 3TU, United Kingdom
Tel: +44 (0) 7552691276
Email: i.minas@lboro.ac.uk

Acknowledgments

The authors would like to express their gratitude to the Engineering and Physical Sciences Research Council (EPSRC) for the sponsorship of this research (EP/N509516/1). Thanks are also extended to Ford Motor Company for the support that was provided for this research.